

Discovering and Generating Hard Examples for Training a Red Tide Detector

Hyungtae Lee^{*†}Heesung Kwon[†]Wonkook Kim[‡]^{*}Booz Allen Hamilton Inc., McLean, VA, USA[†]U.S. Army Research Laboratory, Adelphi, MD, USA[‡]Korea Institute of Ocean Science and Technology, Busan, South Korea

Abstract

Currently, accurate detection of natural phenomena, such as red tide, that adversely affect wildlife and human, using satellite images has been increasingly utilized. However, red tide detection on satellite images still remains a very hard task due to unpredictable nature of red tide occurrence, extreme sparsity of red tide samples, difficulties in accurate groundtruthing, etc. In this paper, we aim to tackle both the data sparsity and groundtruthing issues by primarily addressing two challenges: i) extreme data imbalance between red tide and non-red tide examples and ii) significant lack of hard examples of non-red tide that can enhance detection performance. In the proposed work, we devise a 9-layer fully convolutional network jointly optimized with two plug-in modules tailored to overcoming the two challenges: i) cascaded online hard example mining (cOHEM) to ease the data imbalance and ii) a hard negative example generator (HNG) to supplement the hard negative (non-red tide) examples. Our proposed network jointly trained with cOHEM and HNG provides state-of-the-art red tide detection accuracy on GOCI satellite images.

1. Introduction

Accurate and timely detection of short-term and long-term variations in naturally occurring phenomena (e.g. red tide, sea fog, yellow dust, etc.) that adversely affect wildlife as well as human is highly critical. For instance, red tide is a toxic microscopic organism that inflicts serious damages to not only near-shore fishery but also large marine ecosystems in general. To investigate how, when, where these harmful natural phenomena occur and spread, many countries launched geostationary satellites closely observing areas of interest surrounding their territory. Accordingly, there have been a number of attempts to detect the harmful natural phenomena by analyzing remotely sensed images [7, 10, 25, 27, 30, 35] from the geostationary satel-

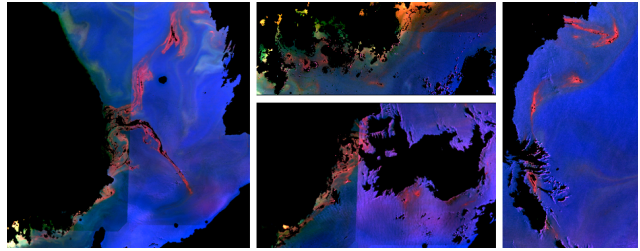


Figure 1: **Red Tide Examples shown on GOCI Images.** In the above figure, red tide appears as elongated red bands.

lites. In this paper, we propose a convolutional neural network (CNN)-based approach that can detect red tide embedded into a large scale image dataset.

To develop a CNN-based red tide detection approach, we have used the large-scale multi-spectral image dataset obtained from GOCI (Geostationary Ocean Color Imager) [4] on a geostationary satellite. Several red tide examples on GOCI multi-spectral images are shown in Figure 1. Since the characteristics of biological properties of red tide do not clearly appear in the image, we used the information on real-world red tide occurrences reported by NIFS (National Institute of Fisheries Science) [1] of South Korea. However, NIFS manually examined red tide occurrence only at a limited number of locations along the southern seashore of South Korea, certainly not being able to cover the entire area infested by red tide. Therefore, in training, we end up with having only a small number of spectral samples from a fraction of areas where red tide actually occur. In our work, we use the images taken in December where red tide do not occur due to the low water temperature as negative examples¹. Figure 2 shows the GOCI images used for the positive (red tide) and negative (non-red tide) training examples, and the red tide region annotation of the positive image.

There are two challenges to use GOCI images and their

¹In South Korea, summer is in July and August and winter in December. Red tide occurs mainly in summer when the water temperature is high.

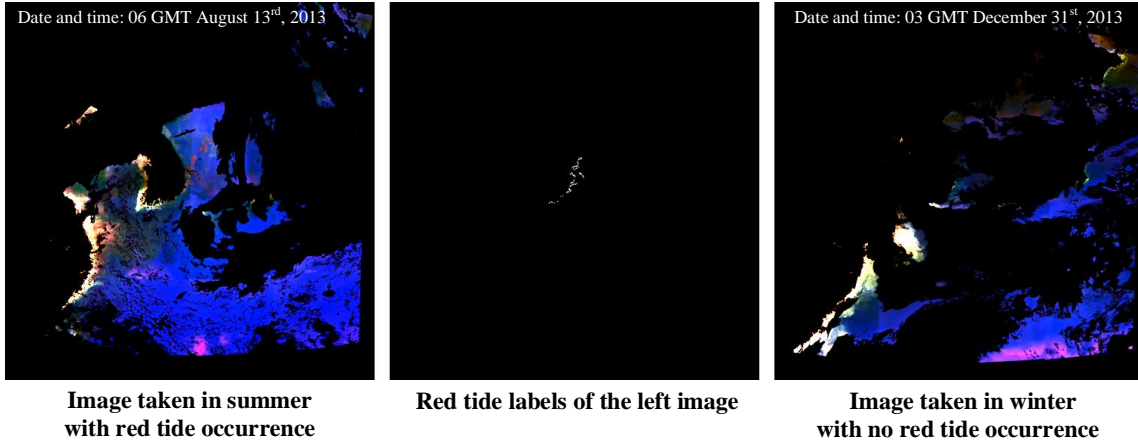


Figure 2: **GOCI Satellite Images and Red Tide Labels.** The images are a false color image by combining the 6th, 4th and 1st band of the GOCI multi-spectral image representing the red, green and blue colors, respectively.

ground truth labels for training the red tide detection. First, the imbalance between the number of positive examples and the number of negative examples is quite significant. The number of positive examples is in the order of one hundred pixels per image, and the number of negative examples is approximately 25M, where each GOCI image has a resolution of 5567×5685 . Since class distributions are significantly unbalanced, the resulting detection model trained on the unbalanced data would be also significantly biased and inaccurate. Second, the spectral characteristics of the images taken in December are very different from those of the images taken in the summer when red tide mostly occurs because the marine environment in summer and winter is very different. Therefore, the negative examples from the December images do not normally represent the non-red tide area from the images collected in summer months. Hence, using the negative examples from the winter season in training may fail to accurately separate the red tide area from non-red tide area in summer images generating a high level of false positives.

In order to cope with a large imbalance between positive examples and negative examples (the first challenge), we adapted the online hard example mining (OHEM) [29] in training the network. Shrivastava et al. introduced OHEM which, for every iteration, sampled a few examples with a high loss from overwhelming examples and use them in training CNN. We used OHEM in a cascaded way to mine a huge volume of negative examples. First, we have taken all positive examples and a randomly chosen subset of negative examples and then apply OHEM to the selected examples to choose hard examples. We called this learning strategy as a *cascaded online hard example mining* (cOHEM).

In order to overcome the second challenge, we implemented a generator based on CNN which artificially creates spectral signals with non-red tide property whose spectral

characteristics are very close to those of red tide examples. This generator is a 4-layered CNN consisting of two convolutional layers and two deconvolutional layers, where input and output of CNN are connected via skip connection. We train the generator in such a way that the generated negative examples are recognized by the red tide detection model as red tide (i.e. false positive). When the generator takes non-red tide examples as input, its output examples are used as hard negative examples in training the red tide detection model. Therefore, this generator is called a *hard negative generator* (HNG).

For the red tide detection model, we implemented a 9-layer fully convolutional network (FCN) inspired by [17]. According to [15, 16, 17], this FCN architecture is suitable for pixel-wise classification in which only a few pixels are annotated as positive examples from the images for training, similar to the red tide detection problem. The network proposed by Lee et al. [17] evaluates each pixel along with local spatial information by applying multi-scale filters to the 5×5 region around the pixel. Since red tide normally covers much larger than the 5×5 region in GOCI image, in order to fully utilize the spatial information in evaluating the red tide pixels, we modified the network so that its receptive field becomes 25×25 .

We conducted several experiments to find out how cOHEM and HNG jointly address the problems that arise in training our network on GOCI images. Experiments confirmed that both modules jointly used together enhance red tide detection performance.

In this paper, we made contributions as follows:

- Use cOHEM to cope with significantly unbalanced class distribution of GOCI images.
- Augment the training dataset by generating hard negative examples via HNG to reduce false alarms.

- Implement a 9 layer FCN jointly optimized with cOHEM and HNG for red tide detection.
- Provides the state-of-the-art red detection accuracy on GOCI images.

2. Related Works

CNN used for Detecting Natural Phenomena in Marine Environment. Since CNN has been introduced and provided promising performance in image classification, there have been several attempts to use it in the marine environment. CNN has been effectively used for detection of coral reefs [20], classification of fish [6], detection of oil from shipwreck [23], and so on. However, applying deep neural network to detect objects-of-interest in the marine environment has been quite limited due mainly to difficulties in acquiring large amounts of annotated data unlike general object detection applications. In this paper, we devise a CNN training strategy coupled with advanced network architecture tailored to red tide detection while minimizing human labeling efforts.

Hard Example Mining. Sung and Poggio [31] firstly introduced hard negative mining (also known as bootstrapping) that trains the initial model with randomly chosen negatives and adapts the model to a hard negatives that consist of false positives of the initial model. Thereafter, hard example mining has been widely used in various applications such as pedestrian detection [2, 5], human pose estimation [3, 18], action recognition [21], event recognition [19], object detection [8, 12, 14, 22], and so on. There are alternative ways to find hard examples using heuristic [11] or other hard example selection algorithms [28, 33], which avoid training multiple times.

Shrivastava et al. [29] introduce online hard example mining which, for every training iteration, carries out hard examples mining that chooses examples with high training loss. However, it is too exhaustive to evaluate all examples on each iteration. Hence, when using a very large example set like our problem, it is impractical to examine all examples for each iteration. Therefore, we use OHEM in a cascaded fashion to randomly select a subset of examples and then perform efficient mining on it.

Training Generator via Adversarial Learning. Szegedy et al. [32] introduce a method to generate an adversarial image by adding perturbation so that it is misclassified by a CNN-based recognition approach. These perturbed images become adversarial images to the recognition approach. Goodfellow et al. [13] introduce two models: a generator that captures the data distribution and a discriminator that estimates the probability that a sample came from the training data rather than the generator. A generator and a dis-

criminator are trained at the same time in a direction to interfere with each other. This is called an adversarial learning framework.

Radford et al. [26] devise an image generation approach based on CNN by adopting this adversarial learning framework. Wang et al. [34] use the adversarial learning framework to train a network that creates artificial occlusion and deformation on images. Object detection network is trained against this adversary to improve performance. We also use the adversarial learning for training hard negative generation network.

3. Red Tide Detection Approach

3.1. Red Tide Detection

In this section, we describe the proposed CNN-based red tide detection algorithm. This approach takes the GOCI image as input and evaluates whether each pixel in the image belongs to a red tide area or not. Therefore, red tide detection can be considered as pixel-wise classification. The architecture of the proposed approach is built on a network introduced by [17], which is known to be suitable for pixel-wise classification. We apply a sliding window method to deal with limited GPU memory when processing GOCI images.

Pixel-wise Classification. Pixel-wise classification is similar to image segmentation in that it clusters pixels with similar characteristics within each category. While the objective loss of image segmentation is calculated by comparing pixel-level labels of the entire image with the output of the network in training, pixel-wise classification is trained to minimize the difference between the labels of several pixels in a local region and their network outputs. In GOCI images, a red tide label is not available for all the red tide pixels, so red tide detection can be treated as a pixel-wise classification problem.

Architecture. The FCN architecture of the proposed approach is shown in Figure 3. The initial module of the network is a multi-scale filter bank followed by two residual learning modules and three convolutional layers (indicated by 7th, 8th, and 9th Conv.), where each residual module consists of two convolutional layers. Dropout layer is attached to the 7th and 8th convolutional layers during training. Batch normalization and ReLU (Rectified Linear Unit) are added to all convolutional layers except for the last layer. The binary sigmoid classifier which is useful for multi-label classification is used for the output layer so that we can perform the tasks of identifying other natural phenomena (e.g. sea fog, yellow dust, etc.) from the GOCI images later with the same architecture.

For red tide detection, the initial multi-scale filter bank

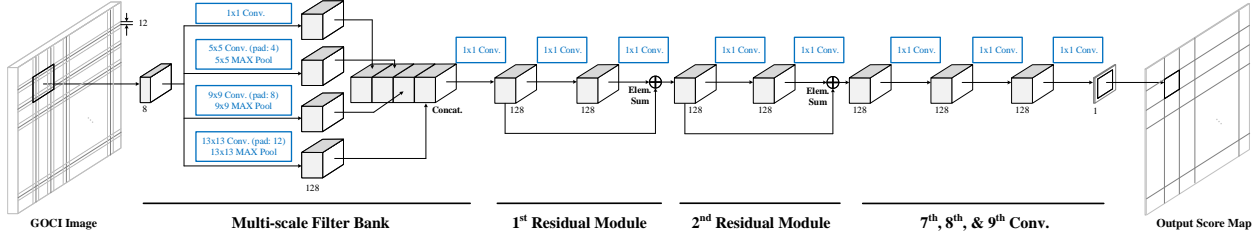


Figure 3: Fully Convolutional Network (FCN) Architecture for Red Tide Detection.

consists of convolutional filters with four different sizes (1×1 , 5×5 , 9×9 , and 13×13). When applying each $k \times k$ filter, the network takes the input image corresponding to $(2k - 1) \times (2k - 1)$ pixels around the evaluated pixel. The input dimension is determined such that each convolution is computed only within the window containing the pixel being evaluated. For example, when applying a 5×5 filter to a 9×9 image, the 5×5 window in the image always contains the center pixel to be evaluated. After the initial convolution, a max pooling layer takes the output from all the convolutional layers except the 1×1 Conv. and outputs the 1×1 feature map. Four feature maps, which are outputs of the initial convolutional layers, are concatenated and fed to the second convolutional layer. The receptive field of the proposed network becomes 25×25 via this multi-scale filter bank and the network uses spatial information from this receptive field in evaluating each pixel.

Sliding Window Strategy. The proposed method cannot process a very large GOCI image at once because of limitations of GPU memory, where the size of the image is 5567×5685 . To overcome this issue, we use sliding window strategy, where each window has $k \times k$ dimension. In our experiment, we set k to 600. Considering our network’s receptive field, only the scores corresponding to the central $(k - 24) \times (k - 24)$ region of the final output are used as a result.

3.2. Training: Adopting cOHEM and HNG

The proposed network is optimized by using a mini-batch Stochastic Gradient Descent (SGD) approach with a batch size of 256 examples, momentum of 0.9, and weight decay of 0.0005. The training objective is to minimize the binary cross entropy losses between the red tide labels and the final output scores. Each batch consists of examples extracted from one positive image with red tide occurrence and one negative image with no red tide occurrence. If both OHEM and HNG are not used for training, the positive-to-negative ratio in each batch is set to 1:3.

To reduce overfitting in training, data augmentation is carried out in training. Since a GOCI image is taken from a top view, training examples are augmented by mirroring across the horizontal, vertical, and diagonal axes. This mir-

roring can be performed in one direction or in multiple directions. This will increase the number of examples by 8 times.

When training the red tide detection network, all learnable layers except the layers of residual modules are initialized according to Gaussian distribution with zero mean and 0.01 standard deviation. The layers of the residual modules are initialized according to Gaussian distribution with a mean of zero and a standard deviation of 0.005.

Cascaded Online Hard Example Mining (cOHEM).

OHEM introduced by Shrivastava et al. [29] builds batches by collecting hard examples to collectively minimize objective loss throughout the entire examples. However, in problems like ours with a very large number of examples, it takes quite long time to find hard examples, so we used OHEM in a cascaded fashion. First, we build a large pool of randomly chosen examples and then carry out OHEM on the pool. This method is called cascaded OHEM (cOHEM).

Figure 4 shows the training protocol of the network using cOHEM. For every pixel labeled with red tide, a 25×25 area around each pixel is collected and used as a positive example. In *Negative Random Sampler*, we randomly select 100 regions of a size 29×29 from a negative image. In our experiments, we found that it is important to randomly select multiple regions instead of one wide region for negative examples, in order to effectively improve the accuracy of red tide detection using cOHEM. For all selected examples, their classification losses are calculated by feeding the examples to the network. Note that this loss represents the extent to which the current network correctly classifies each example. *Hard Example Sampler* randomly selects the high loss examples with predetermined batch size. Then the proposed network is trained with these batches consisting of hard examples. Then, the proposed network is trained by constructing these batches with hard examples.

Hard Negative Generator (HNG).

We introduce a hard negative generation (HNG) network that generates hard negatives that are likely classified by the red tide detection network as false positives. We train the proposed network on these artificially generated hard negatives to primarily

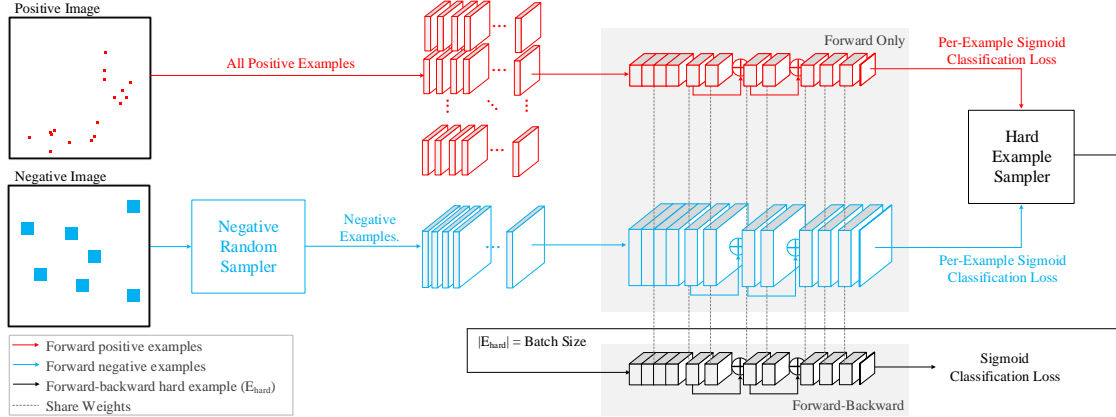


Figure 4: **Training Red Tide Detection Network by using Cascaded OHEM (cOHEM).** cOHEM finds hard examples through two-stage sampling (*Negative Random Sampler* and *Hard Example Sampler*) for every iteration.

reduce false positives. For the HNG architecture, we implement a 4-layered network consisting of two convolutional layers and two deconvolutional layers, which is inspired by conv-deconv network [9, 24], as shown in Figure 5. The input and output of HNG network are connected by skip connection. All the layers use 3×3 filters. Batch normalization and ReLU are added to the end of the first three layers of the network. In [26], deconv network which takes a high-dimensional feature map with a small spatial dimension and outputs a low-dimensional map with a large spatial dimension is proven to be effective for image generation. Unlike [26], our generator takes a negative example as an input instead of a one-dimensional random signal to preserve characteristics of actual negative examples via the skip connection.

We trained the HNG network to maximize red tide detection loss on hard negatives generated, which contrasts with the red tide detection network’s objective. In other words, these generated hard negatives are adversarial examples to deceive the red tide detection network. Mathematically, we assume that the red tide detection network and its loss are represented by \mathcal{F}_r and $\mathcal{L}_{\mathcal{F}_r}$, respectively. Red tide detection network is trained by minimizing its loss which is expressed as:

$$\mathcal{L}_{\mathcal{F}_r}(E, L) = \mathcal{L}_{cross-entropy}(\mathcal{F}_r(E), L), \quad (1)$$

where E and L are training examples and their associated red tide labels, respectively. For each example $e \in E$, its red tide label $l_e \in L$ can be either 1 (red tide) or 0 (non-red tide).

The objective of HNG (denoted by \mathcal{F}_{hng}) is to generate a negative example incorrectly classified as red tide by red tide detection network. Accordingly, HNG loss can be expressed as:

$$\mathcal{L}_{\mathcal{F}_{hng}}(N) = \mathcal{L}_{\mathcal{F}_r}(\mathcal{F}_{hng}(N), \mathbf{1}), \quad (2)$$

where N is a set of real negative examples. $\mathbf{1}$ indicates that labels associated with the generated negative examples are red tide. HNG can be trained by minimizing $\mathcal{L}_{\mathcal{F}_{hng}}(N)$, where $\mathcal{F}_{hng}(N)$ becomes adversarial examples for the red tide detection network.

For training the red tide detection network with hard negatives generated by HNG, we adopt a 3-stage training algorithm. The first stage is to train the red tide detection network. In the second stage, HNG is trained while keeping the red tide detection network weights fixed, as shown in Figure 5. All layers of HNG are initialized according to Gaussian distribution with a mean of zero and a standard deviation of 0.02. In the last stage, the red tide detection network is updated by using examples generated by HNG along with real examples.

4. GOCI Satellite Images

GOCI (Geostationary Ocean Color Imager) acquires multispectral images from a large area surrounding the Korean peninsula. The GOCI image [4] has 8 channels consisting of 6 invisible and 2 near infrared (NIR) frequency bands and 500 m spatial resolution. The size of the GOCI image is 5567×5685 . Some examples of GOCI images are shown in Figure 2.

In this paper, we use GOCI images taken in July, August, and December of 2013 to evaluate our red tide detection network. Images of July and August where red tide occurred are used as positive images and December images are used as negative images. Considering some conditions such as the atmosphere, we chose 8 images in July and August and 4 images in December. Half of them were used for training and the other half for testing.

In order to label red tide pixels where red tide actually occurs, we used the red tide information reported by NIFS (National Institute of Fisheries) of South Korea written after

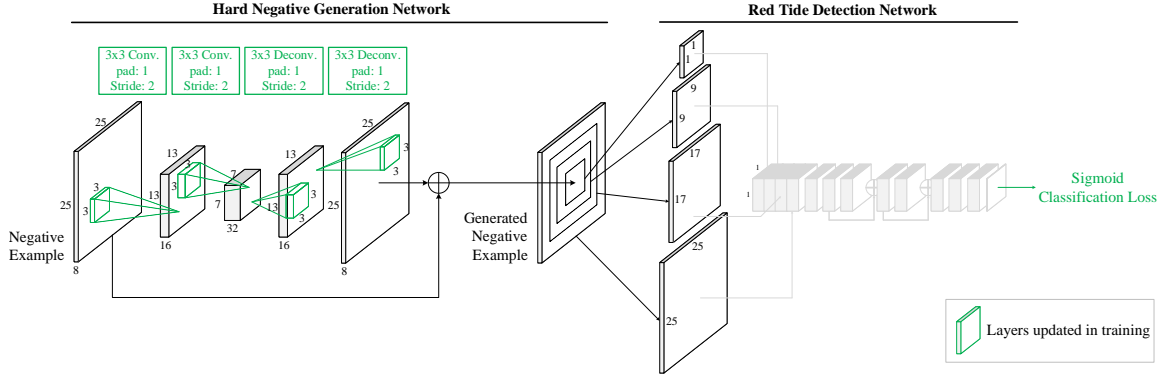


Figure 5: **Training Hard Negative Generation (HNG) Network.** The faded network is a red tide detection network and its weights are not updated when training a hard negative generation network.

directly testing seawater from a ship. However, NIFS examined red tide occurrence from a limited number of locations; it is actually impossible to cover the entire red tide areas. Furthermore, the red tide positions indicated in the report were also not very accurate due to the error-prone manual process that includes mapping geo-coordinates of red tide locations onto GOCI images. Hence, we have extended potential red tide regions up to 25 km (50 pixel distance) in all directions from the red tide location indicated in the report and then labeled red tide with the help of experts. Approximately 100 pixels from each training image were sparsely labeled as a red tide area. We used pixels labeled as red tide as positive examples and all the pixels of December images as negative examples.

5. Experiments

5.1. Evaluation Settings

Evaluation Metrics. We used two different metrics for the evaluation of the proposed network: the receiver operating characteristic (ROC) curve and the ROC variation curve. The ROC variation curve describes changes in the detection rate based on varying numbers of (true or false) detections per image (NDPI) instead of the false positive rate. This metric is especially useful when there are numerous unlabeled samples whose identity is unknown. Note that in a GOCI image only a fraction of red tide pixels are labeled and the rest of the image remains unlabeled. For quantitative analysis, we calculate the AUC (the area under the ROC curve) and $\text{ndpi}@dr=0.25$, $\text{ndpi}@dr=0.5$ and $\text{ndpi}@dr=0.75$ indicating the NDPI values when the detection rate reaches 0.25, 0.5, and 0.75, respectively.

Network Training. The proposed networks are trained from scratch. When both cOHEM and HNG are used for training, we used a three-stage training strategy and trained the network with 1250 iterations for each stage. A base

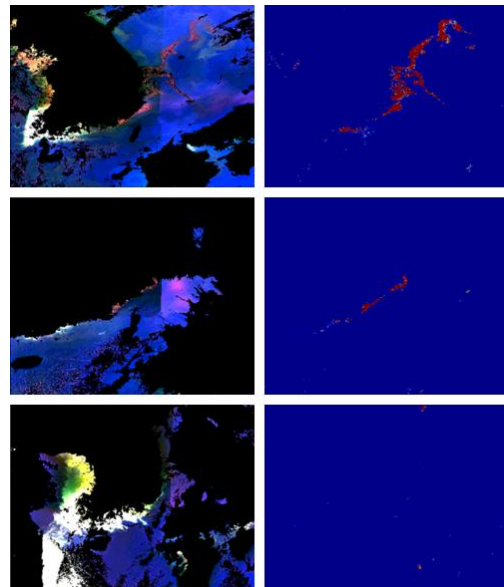


Figure 7: **Red Tide Detection Results.** The left images and the right images are input images and the corresponding red tide detection results, respectively, from our approach. The first and second input images have red tide in them and the last image is a negative image without red tide.

learning rate is 0.01 and dropped by 10 for every 500 iteration. When the three stage training strategy is not used to train the network (i.e. both cOHEM & HNG are not adopted for training), we trained the network with 2500 iterations. A base learning rate is 0.01 and dropped by 10 for every 1K iteration.

5.2. Experimental Results

Baselines. We implement two baselines of SVM and CNN-based hyperspectral image classification approach [17] by which our network is inspired. In SVM, a 25×25 region centered on the pixel in test is used as a feature representing

Method	AUC (%)	ndpi@dr=0.25	ndpi@dr=0.5	ndpi@dr=0.75
SVM	81.0	295732	4641404	34863121
+ Hard Negative Mining	82.4	114067	1259805	5313930
[17]	84.9	39431	168778	636537
+ cOHEM	87.5	28165	125020	367485
+ cOHEM & HNG	88.9	17884	71360	260716
Ours	90.6	8477	33755	134479
+ cOHEM	93.3	8555	31873	79584
+ cOHEM & HNG	97.3	6282	18905	58352

Table 1: **Red Tide Detection Accuracy.** For each metric, **numbers in bold** indicate the best accuracy. Note that the higher the AUC value, the better the performance, and the smaller the value of NDPI, the better the performance.

the center pixel. In order to know the advantages of adopting hard example mining, we applied conventional hard negative mining [31] to SVM training.

Performance Comparison. Table 1 shows that our network trained by searching hard examples (via cOHEM) and generating hard negatives (via HNG) provides the highest accuracy in all four metrics. Overall, AUC is relatively high, as most of the negatives from negative images are easy to detect which leads very low false alarm rate. Therefore, the metrics of ndpi@dr are much more meaningful since they represent critical red tide detection performance in positive images. We also found that adopting a hard example mining approach consistently improves the accuracy of all three methods. Adopting the HNG network was also effective in improving the performance of our network and [17].

Figure 6 shows the ROC variation curves for our network and baselines. Based on the curves, we can confirm that our network provides significantly enhanced detection performance over other techniques over the entire range of NDPI. In particular, our network misses much fewer positives than other baselines, which is highly critical in red tide detection. Figure 7 shows red tide detection results from our approach.

5.3. Finding the Network Specification

In order to find the optimal specification of the proposed network, we evaluate the network by changing the number of filters, the number of residual modules, and the type of filter used in multi-scale filter bank. The proposed network specifications are determined after evaluating detection accuracy with AUC, training time, and test time. These evaluations and determined network specifications are shown in Table 2. Table 2 shows that if the network is enlarged by increasing the depth and breadth of the network, training of

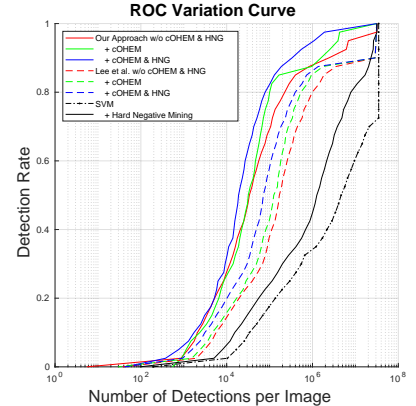


Figure 6: **ROC Variation Curve.** To better view changes of detection rate and NDPI in detail, the x axis is shown with logarithmic scale.

the network may be overfitted on GOCI dataset.

5.4. Finding Sampling Strategy of cOHEM

We compare various negative example sampling strategies of cOHEM with respect to detection accuracy and training time. Negative example sampling can change based on two factors: a negative window size and the number of negative windows. In Table 3, we compare four different sampling strategies with different factors. The last strategy sampling 256 negative windows with size 25×25 is training without adopting cOHEM. Since the fourth method is not using cOHEM separately, its training time is the shortest.

In Table 3, the first two methods of sampling the most negative examples do not provide better performance than the third method. This observation indicates that increasing spatial diversity of sampling is important in providing competitive performance. Therefore, even though the third method requires large memory and provides the smaller number of examples, it is adopted in our training approach.

5.5. Analyzing HNG Network

Figure 8 presents different sets of negative training examples, each set includes real negative examples (left) and the corresponding generated negative examples (center). Note that the red tide detection network found no false alarms from the real negative examples but detected some false alarms from the generated examples, which are in turn used as hard negative examples. These generated hard negative examples can be selected when the second training phase of a three-step training strategy is completed. As previously explained, the red tide detection network is re-adapted on the false-positive generated examples at the third training stage.

In Figure 8, we can observe that the generated negative

	64	96	128	192		1	2	3		1×1	$\sim 5 \times 5$	$\sim 9 \times 9$	$\sim 13 \times 13$
AUC (%)	82.2	86.5	90.6	90.7	AUC (%)	81.7	90.6	90.6	AUC (%)	87.6	88.7	89.7	90.6
Train (min)	42.0	49.1	56.4	62.5	Train (min)	47.5	56.4	63.1	Train (min)	37.5	40.5	47.5	56.4
Test (sec/im)	13.4	16.2	18.3	20.5	Test (sec/im)	16.0	18.3	21.4	Test (sec/im)	11.3	12.5	14.3	18.3
(a) # of filters of each layer				(b) # of residual module				(c) Multi-scale filter bank.					

Table 2: **The Optimum Specification of the Network.** The network specification is determined according to three metrics: detection accuracy (AUC), training time, and test time. Titan XP is used as a GPU that affects training time and test time. **Numbers in bold** indicate specifications used in our network. Notation: $\sim 13 \times 13$ means the multi-scale filter bank consisting of 1×1 , 5×5 , 9×9 , and 13×13 convolutional filters.



Figure 8: **Generated Training Examples.** Each set consists of three images: real negative example (left), generated negative example (center), and red tide network activation in the generated example (right). White pixels in the activation map indicate pixels with a red tide score estimated by the red tide detection network greater than 0.5. For every set in this figure, there was no activation for a real negative example.

Neg. window size	101	45	29	25
# of window	1	10	100	192
# of pixels	10.2K	20.3K	84.1K	120.0K
# of examples	5.9K	4K	2.5K	192
AUC (%)	90.7	90.2	93.3	90.6
Train time (sec/iter)	0.521	0.534	0.540	0.482

Table 3: **Accuracy vs Hard Negative Sampling Strategy of cOHem.** Numbers in bold indicate our cOHem sampling strategy. A negative map dimension of k indicates the $k \times k$ map.

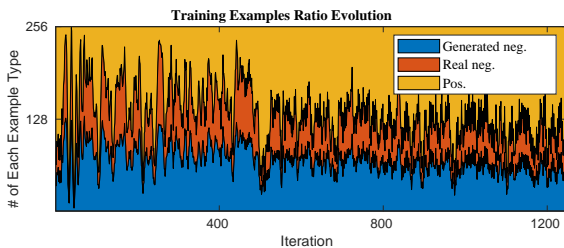


Figure 9: **Training Example Ratio Evolution.** This evolution shows the change in training example ratio at the third stage of the training strategy.

examples and the real negative examples used as input to the HNG network are similar to each other, so it is not easy to distinguish them. This means that while the generated examples mostly maintain the characteristics of their corresponding real examples, the slight differences created by the HNG network convert the real examples to hard negative

examples. Another interesting observation from Figure 8 is that most of the generated hard negative examples are located in the red area where red tide does not actually occur.

Figure 9 shows an evolution of the change in training example ratio among positive examples, real negative examples, and generated hard negative examples within one batch as the training progresses. Overall, the proportion of generated hard negative examples in a batch gradually decreases as the training iteration increases. However, its difference between the beginning and the end of training is not large. This observation indicates that HNG network generates examples that are difficult for the red tide detection network to detect, hence named hard negative examples, regardless of the training state of the red tide detection network.

6. Conclusion

In this paper, we have developed a novel 9-layer fully convolutional network for red tide detection on GOCI satellite images. Even though the GOCI dataset is a large scale set of multispectral images, the dataset suffers from extreme data sparsity of red tide samples, data imbalance between positive and negative samples, and lack of hard negative samples. To cope with significant data imbalance of GOCI images, we adopt cOHem, which selects hard examples from a very large-scale set of examples, for training the network. We also implement a hard negative generator (HNG) to supplement hard negatives to training examples. The proposed FCN jointly trained with cOHem

and HNG provides the state-of-the-art accuracy for red tide detection.

Acknowledgement. This research was supported by the “Development of the integrated data processing system for GOCI-II” funded by the Ministry of Ocean and Fisheries, Korea.

References

- [1] <http://www.nifs.go.kr/redtideInfo/>. 1
- [2] L. Bourdev, S. Maji, T. Brox, and J. Malik. Detecting people using mutually consistent poselet activations. In *ECCV*, 2010. 3
- [3] L. Bourdev and J. Malik. Poselets: Body part detectors trained using 3D human pose annotations. In *ICCV*, 2009. 3
- [4] S. Cho, Y. Ahn, J. Ryu, G. Kang, and H. Youn. Development of Geostationary Ocean Color Imager (GOCI). *Korean Journal of Remote Sensing*, 26(2):157–165, 2010. 1, 5
- [5] N. Dalal and B. Triggs. Histograms of oriented gradients for human detection. In *CVPR*, 2005. 3
- [6] G. Ding, Y. Song, J. Guo, C. Feng, G. Li, B. He, and T. Yan. Fish recognition using convolutional neural network. In *OCEANS*, 2017. 3
- [7] L. Dong, B. Wang, M. Zhao, and W. Xu. Robust infrared maritime target detection based on visual attention and spatiotemporal filtering. *IEEE Transactions on Geoscience and Remote Sensing (TGARS)*, 55(5):3037–3050, 2017. 1
- [8] P. Felzenszwalb, R. Girshick, D. McAllester, and D. Ramanan. Object detection with discriminatively trained part based models. *IEEE Transactions on Pattern Analysis and Machine Intelligence (TPAMI)*, 32(9):1627–1645, 2010. 3
- [9] D. Fourure, R. Emonet, E. Fromont, D. Muselet, A. Tremeau, and C. Wolf. Residual conv-deconv grid network for semantic segmentation. In *BMVC*, 2017. 5
- [10] A. Germán, C. Tauro, M. Scavuzzo, and A. Ferral. Detection of algal blooms in a eutrophic reservoir based on chlorophyll-a time series data from MODIS. In *IGARSS*, 2017. 1
- [11] R. Girshick. Fast R-CNN. In *ICCV*, 2015. 3
- [12] R. Girshick, J. Donahue, T. Darrell, and J. Malik. Region-based convolutional networks for accurate object detection and segmentation. *IEEE Transactions on Pattern Analysis and Machine Intelligence (TPAMI)*, 38(1):142–158, 2016. 3
- [13] I. Goodfellow, J. Pouget-Abadie, M. Mirza, B. Xu, D. Warde-Farley, S. Ozair, A. Courville, and Y. Bengio. Generative adversarial nets. In *NIPS*, 2014. 3
- [14] K. He, X. Zhang, S. Ren, and J. Sun. Spatial pyramid pooling in deep convolutional networks for visual recognition. *IEEE Transactions on Pattern Analysis and Machine Intelligence (TPAMI)*, 37(9):1904–1916, 2015. 3
- [15] H. Lee, S. Eum, and H. Kwon. Cross-domain CNN for hyperspectral image classification. In *IGARSS*, 2018. 2
- [16] H. Lee and H. Kwon. Contextual deep CNN based hyperspectral classification. In *IGARSS*, 2016. 2
- [17] H. Lee and H. Kwon. Going deeper with contextual CNN for hyperspectral image classification. *IEEE Transactions on Image Processing (TIP)*, 26(10):4843–4855, 2017. 2, 3, 6, 7
- [18] H. Lee, V. Morariu, and L. Davis. Qualitative pose estimation by discriminative deformable part models. In *ACCV*, 2012. 3
- [19] H. Lee, V. Morariu, and L. Davis. Clauselets: Leveraging temporally related actions for video event analysis. In *WACV*, 2015. 3
- [20] A. Mahmood, M. Bennamoun, S. An, F. Sohel, F. Boussaid, R. Hovey, G. Kendrick, and R. Fisher. Coral classification with hybrid feature representations. In *ICIP*, 2016. 3
- [21] S. Maji, L. Bourdev, and J. Malik. Action recognition from a distributed representation of pose and appearance. In *CVPR*, 2011. 3
- [22] T. Malisiewicz, A. Gupta, and A. Efros. Ensemble of exemplar-SVMs for object detection and beyond. In *ICCV*, 2011. 3
- [23] M. Nieto-Hidalgo, A.-J. Gallego, P. Gil, and A. Pertusa. Two-stage convolutional neural network for ship and spill detection using SLAR images. *IEEE Transactions on Geoscience and Remote Sensing (TGARS)*, 56(9):5217–5230, 2018. 3
- [24] H. Noh, S. Hong, and B. Han. Learning deconvolution network for semantic segmentation. In *ICCV*, 2015. 5
- [25] B. Pan, Z. Shi, Z. An, Z. Jiang, and Y. Ma. A novel spectral-unmixing-based green algae area estimation method for GOCI data. *IEEE Journal of Selected Topics in Applied Earth Observations and Remote Sensing (JSTARS)*, 10(2):437–449, 2017. 1
- [26] A. Radford, L. Metz, and S. Chintala. Unsupervised representation learning with deep convolutional generative adversarial networks. In *ICLR*, 2016. 3, 5
- [27] A. Rahman and A. Aslan. Detecting red tide using spectral shapes. In *IGARSS*, 2016. 1
- [28] S. Ren, K. He, R. Girshick, and J. Sun. Faster R-CNN: Towards real-time object detection with region proposal networks. *IEEE Transactions on Pattern Analysis and Machine Intelligence (TPAMI)*, 39(6):1137–1149, 2017. 3
- [29] A. Shrivastava, A. Gupta, and R. Girshick. Training region-based object detectors with online hard example mining. In *CVPR*, 2016. 2, 3, 4
- [30] H. Su, O. Olasimoju, Y. Yong, L. Yang, H. Liang, and W. Wang. Detection of red tide using Aqua-Terra MODIS satellite data for Aransas bay, Texas. In *IGARSS*, 2016. 1
- [31] K. Sung and T. Poggio. Learning and example selection for object and pattern detection. In *MIT A.I. Memo*, number 1521, 1994. 3, 7
- [32] C. Szegedy, W. Zaremba, I. Sutskever, J. Bruna, D. Erhan, I. Goodfellow, and R. Fergus. Intriguing properties of neural networks. In *ICLR*, 2014. 3
- [33] J. Uijlings, K. van de Sande, T. Gevers, and A. Smeulders. Selective search for object recognition. *International Journal of Computer Vision (IJCV)*, 104(2):154–171, 2013. 3
- [34] X. Wang, A. Shrivastava, and A. Gupta. A-Fast-RCNN: Hard positive generation via adversary for object detection. In *CVPR*, 2017. 3

[35] J. Zhao, H. Ghedira, and M. Temimi. Remote sensing of red tide in the Arabian Gulf. In *IGARSS*, 2014. 1